FINAL REPORT

Contract NAS 9-8869

"Supporting Studies for the Coronagraph Contamination Experiment"

Period: September 1, 1968 to February 28, 1971

Prinicipal Investigator: Natalie S. Kovar
University of Houston
Houston, Texas

A. INTRODUCTION

In accordance with the aims specified in the contract, the following tasks were completed by the Contractor in the allotted time period (September 1, 1968, to February 28, 1971):

(1) Calculation of Mie Scattering Functions.

(a) Computation of individual particle scattering functions. These calculations were done for a range in particle size and a range in the wavelength of incident light. In particular, computations were completed for a 15Å particle and for particles subjected to incident light of ultraviolet wavelengths as specified in the contract. A list of computed individual particle scattering functions is given in Appendix A. (Here λ is the wavelength of incident light, α is 2π x the ratio of particle size to the wavelength of incident light.)

(b) Computation of Mie Scattering Functions for a Mixture of Particles.

These have been done for a range in α of 2 to 240 (as specified in the contract) and for a number of other particle distributions. They are listed in Appendix B.

The calculations cited in (a) and (b) necessitated an assessment as to demands on computer memory, storage and computational time. Though some of the calculations were carried out on a Sigma 7, the vast majority were done on the Univac 1108. A duplicate copy of the appropriate deck written on Fortran 5 can be made available upon request.

(2) Calculations of Contaminant Atmospheres for Gemini, Apollo and SKYLAB.

These have involved assumptions as to the leakage rates for the respective vehicles and, thus, of the mass column density of the atmospheres surrounding them. Atmospheres for these vehicles have been computed for the two cases specified in the contract; namely,

(a) a uniform particle size distribution.

(b) a particle distribution in which size varies as r^{-3}.

Results of these computations are presented in the body of this report.

B. MIE SCATTERING FUNCTION CALCULATIONS

During the contract period, the relative Mie scattering functions, $\sigma(\theta)$ where θ is the scattering angle, were computed for spherical particles having an index of refraction m and a size distribution $n(r) \propto r^{-k}$, r being particle size, and k the distribution function. In the case where k=0, of course, all particles are of the same size. Results of the calculations of scattering functions for an individual scattering particle are presented first, followed by scattering functions for a distribution of particles of varying size.

(1) Individual Scattering Functions.

The evaluation of the scattering function involves a series expression consisting of Riccati-Bessel functions, which may have a complex argument, and derivatives of Legendre polynomials. (We have compiled and printed out tables of Riccati-Bessel functions though in our calculation of the scattering function, these are not printed out separately.)

The convergence of the series requires a number of terms slightly greater than α. This results in computational time increasing rapidly with particle size.

Now, contributions to the contamination atmosphere may be either controlled or continuous. Continuous contributions give rise to scattering by a column of various sized particles. Controlled events such as waste dumps or thruster firings, however, result in light being scattered by individual large particles. Thus, for the spacecraft contamination problem, scattering functions appropriate to scattering by individual spherical ice particles have been calculated. The range in particle size considered is 15Å to 1 cm and the wavelength of incident light ranges from 1000Å to 5300Å.

Figure 1 shows the scattering curve for a 15Å particle with an index of refraction m = 1.33 subject to incident light of 5300Å (representative of visible light). The ordinate is the log of the scattering function and the abscissa the scattering angle. σ_1 is the scattering function for the component of the incident plane wave having its electric vector perpendicular to the plane of vision and σ_2 that for the electric vector parallel to the plane of vision. $\bar{\sigma}$ is the average of the two. Figure 2 is the scattering function for a 15Å particle for incident light of 1200Å, which is in the vacuum ultraviolet near the Lyman α line. The index of refraction of ice at this wavelength is complex and equal to 1.333 - 0.4414 i. Note that for both wavelengths, the curves are smooth and σ_2 has a pronounced minimum at 90°. This means, of course, that strong polarization occurs at this angle.

Figure 3 gives the scattering curves for a 1μ size particle for incident light of 5300Å, represented by the solid line, and of 2500Å, represented by the dashed line. The two curves are similar, consist of many maxima and minima, and differ markedly from those for 15Å. For small scattering angles, $\theta < 10°$, the values of the scattering function at the two wavelengths differ significantly, but for larger scattering angles, the scattering functions have approximately the same value. The curve for a 1μ particle at 1200Å is shown in Figure 4. Here the index of refraction is complex and the curve differs from those at 5300Å and 2500Å in that it damps out at about 90°. Figure 4 illustrates a portion of the scattering curve, σ_1, for a 1000μ particle for incident light of 5300Å. The interval of scattering angle shown is 140° to 140.2°. To obtain the exact curve for this size particle, increments in theta must be of the order of 0.002. With such increments, or even smaller ones as for the case of a 1 cm particle where $\Delta\theta = 0.0002$ is required, machine time becomes prohibitive. Consequently for the larger particles, 10 or more microns, an averaging or sampling technique was devised and the value of the scattering function computed at selected values of the scattering angle. The procedure used was to compute the scattering function at certain specified intervals in theta. Then, at each of these values the scattering function was calculated at a selected number of adjacent angles and the average scattering function computed for the proscribed range in scattering angle. Figure 5 compares the actual and sampled values of $\bar{\sigma}$ for a 10μ particle at 5300Å. The solid line is for the sampled values, and the x's the actual values as taken

from the detailed scattering curve. The agreement is quite good.

Figure 6 shows the sampled curve for a 100μ particle for incident light of 2500Å. The many maxima and minima of the detailed curve have been smoothed out, but the essential shape of the curve has been retained. There are strong secondary maxima at about 120° and 140°. The latter is typical of ice particles. As the next figure (Figure 6) indicates, when the index of refraction becomes complex, as it does for ice at λ=1200Å, the scattering curve exhibits a substantially different behavior. The curves in this figure are for a 10μ particle. σ_1 no longer has a pronounced maximum at 140°, but increases slowly to a maximum at 100°. σ_2 has a rather broad maximum from 60° to 90°.

(2) Mie Scattering Functions for Particles Heterogeneous in Size.

The relative Mie scattering functions, $\sigma'(\phi)$, for spherical particles having an index of refraction m and following a size distribution $n(r) \propto r^{-k}$ were computed. The total scattering function is related to the relative scattering function by

$$\sigma(\theta) = C \int_{\alpha_{min}}^{\alpha_{max}} [i_1(\alpha,\theta) + i_2(\alpha,\theta)]\alpha^{-k} d\alpha$$

where C is normalizing factor and i_1 and i_2 are the individual particle scattering functions discussed is section (1) above. Figure 7 shows the relative scattering function for a distribution of 12 to 120 in α with m = 1.33 and k, the distribution function, equal to 2.5. Increments in alpha, $\Delta\alpha$, equal 0.10.

For λ=5300 Å, this range in α corresponds to a particle size range of 1 to 10μ. This particle size interval is an appropriate selection for the spacecraft contamination problem. For particles of size much smaller than 1μ, the scattering approaches Rayleigh scattering and particles much larger than 10μ tend to scatter as random individuals and would not appreciably contribute to the general background radiance. Note that the many maxima and minima of the individual scattering functions have been smoothed out leaving a prominent maximum at 140°.

Figure 8 shows the relative scattering function for the same k and m, but for a particle distribution function in alpha of 12 to 240. That is, r ranges from 1 to 20μ for a wavelength of 5300 Å.

Though the calculations presented are for ice particles, the program is written in a general form and will accommodate any m or α within machine capacity.

C. CONTAMINANT ATMOSPHERE CALCULATIONS

The quantity of interest to be calculated is the radiance of the contaminant cloud, B. If light scattering is considered to be done by a column of particles, either of uniform size or varying in size, the radiance of the cloud in terms of the Sun's mean surface brightness, $B_\odot$, is

$$B/\overline{B}_\odot \approx \Omega_\odot \, \sigma(\varepsilon) M_s$$

where $\Omega_\odot$ is the solid angle subtended by the Sun at the spacecraft, $\sigma(\varepsilon)$ is the mass scattering coefficient (ε is the elongation), and M_s is the mass column density.

Assuming that a particle of radius r leaves the spacecraft radially with a velocity v_o, an expression for the mass loss rate dm/dt can be derived. Since at the altitudes of interest the most effective mechanism of particle removal is aerodynamic drag, and since even this mechanism is relatively unimportant, the column of material extends out to a distance R_1 from the spacecraft of radius R_o (where $R_1 > R_o$). If we represent the Gemini and Apollo spacecraft by a sphere of radius R_o and assume that there is a uniform space density of particles surrounding these spacecraft, then the column mass density of material, M_s, is

$$M_s = \frac{1}{4\pi R_o v_o} \left[dm/dt\right]_{H_2O} \quad gm/cm^2 .$$

The ATM (or Skylab) configuration must be treated in a slightly different manner since it resembles a cylinder of radius R_o and length L. If it is assumed that the amount of material outgassed at the ends of the cylinder is small compared to the amount outgassed along its length, then the column mass density associated with ATM can be found using an analysis similar to that used for the spheres of Gemini and Apollo. For ATM

$$M_s = \frac{1}{2\pi L v_o} \left[dm/dt\right]_{H_2O} \ln R_1/R_o \quad gm/cm^2 ,$$

where R_o is the radius of the S-IV B stage and L is approximately 3×10^3 cm.

The total continuous leakage rates as well as the value of R_o and that of the mass column density for Gemini 3 and 11, Apollo and the ATM cluster are presented in Table I. The leakage rates for the Gemini spacecraft were obtained from the Cape Kennedy Archives and represent the maximum and minimum rates for the Gemini vehicles as experimentally determined prior to the launch of each vehicle. The values adopted for Apollo and the ATM cluster are estimates obtained from the Crew Systems Division of the Manned Spacecraft Center. Of interest, though, is not the total leakage rate but that for water vapor. The percentage water vapor can be estimated from the known temperature and relative humidity of the cabin atmosphere--about 293°K and 60% respectively. In computing the mass column density of particles it was assumed that all of the water vapor leaking out of the spacecraft emerges as ice particles or forms ice particles shortly after exhaust. In order to estimate the velocity of the escaping material, conditions in and around the spacecraft must be examined. Inside the vehicle, gas is under 1/3 atmosphere, while outside a near vacuum exists. Gas flow through leaks in the walls of the spacecraft can be considered to resemble flow through a supersonic wind tunnel. Such an analysis gives for the lower limit for the exhaust velocity that of the speed of sound at the cabin temperature, 3.3×10^4 cm/sec. This value was adopted for the computations presented in this report.

It may be that not all the escaping water will condense into micron sized particles but that a large percentage of the resultant particles will be Angstrom sized. Also, the assumption of a smooth distribution of particle radii [$n(r) \propto r^{-k}$] may not represent the actual situation at all. Some supersonic wind tunnel experiments with humid water, for example, suggest that the ice particles formed in the expansion would be uniform in size and of the order of 15 Å. Figure 9 shows how the radiance of a cloud of 15 Å particles having an index of refraction of 1.33 varies with distance from the Sun for incident light of 5300 Å. The ordinate is the radiance in units of the mean solar radiance and the abscissa is the elongation. The solid line is the 15 Å curve and the dashed line the radiance curve for the outer corona and the zodiacal light as determined by Blackwell and Weinberg, respectively (see references). The distribution function is, of course, equal to zero. As is to be expected, such a cloud would not be very bright and would not hamper coronal or zodiacal light observations.

Figure 10 shows the radiance curves for a cloud of 10μ and a cloud of 100μ particles surrounding the ATM for light of 5300 Å. The solid line is the 10μ curve, the dashed line the 100 μ curve and the long followed by a short dashed line the zodiacal light. Note that the curve for the 10μ particles falls below that for the zodiacal light for small elongations, $\varepsilon \lesssim 20°$, where it starts to exceed the brightness of the zodiacal light and continues to do so to about 60° elongation. It then falls well below the zodiacal light except for a small

range in elongation around 140°. The 100μ curve stays well below that for the zodiacal light except for a narrow range in elongation around 140°.

It is of interest to ascertain the effect of the debris in the ultraviolet. Figure 11 shows the curves for the intensity of scattered light, expressed in Rayleighs, due to a 10μ and a 100μ cloud surrounding ATM. Again, the 10μ cloud is brighter than the 100μ cloud.

Figure 12 shows the radiance curves for two different types of particle distributions. The radiance of a debris cloud of 1μ particles surrounding the ATM is given by the dashed line and that of a cloud composed of particles ranging in size from 0.2 to 20μ and having a distribution of 2.5 by the solid line. In both cases an index of refraction equal to 1.33 was assumed. The 1μ cloud is brighter than the zodiacal light for all elongations larger than about 5°. The situation is even worse for the mixture of particle sizes. Here the radiance curve is above that for the zodiacal light for all elongations and is of the order of 10^{-9} to 2.4×10^{-12} $\overline{B}_{\odot}$ for all angles larger than 10°, making daylight observations of the zodiacal light impossible.

It is of interest to see how the radiance curve is affected when the scattered earthlight is taken into account. Figure 13 shows the radiance of a debris cloud surrounding Gemini 11 with and without the earthlight contribution. Calculations for scattered earthlight were carried out in this case for the

spacecraft located over the terminator. For elongations less than about 20°, the contribution of scattered earthlight is not important. In the elongation interval 40° to 180°, scattered earthlight sets a background brightness of about $10^{-10}\ \overline{B}_{\odot}$. Disregarding the angular interval of backscattered earthlight, the background radiance for GT-11 would be about $10^{-12}\ \overline{B}_{\odot}$ for this same range in elongation. The debris cloud both in this figure and in the next was assumed to be composed of particles having a size range of 0.2 to 10μ, with a distribution function of 3 and an index of refraction of 1.30.

Figure 14 shows the calculation for Apollo and ATM. This figure shows quite graphically that daylight observations will probably not be feasible for ATM (Skylab) unless stringent precautions are taken about waste dumps, thruster firings, cabin leaks, etc. Again, though, the assumptions that have been made must be stressed: the leakage rates are uncertain, the exact size distribution and state of the debris is uncertain, the ejection velocity is uncertain.

The computer program for the calculation of the contaminant atmospheres is written in the format--constant x scattering function x mass column density--and so may be used for other particle distributions and other mass column densities than specified above.

D. PUBLICATIONS

Several publications have resulted from the work carried

out under this contract. These have been reported in (and copies of the publications attached to) the monthly progress reports.

References

1. D. E. Blackwell, Mon. Nat. R. Astr. Soc. 115, 629 (1955).

2. N. S. Kovar, "Theory of Light Scattering by Manned Spacecraft Atmospheres," invited paper presented at Symposium for Optical Contamination in Space, August 1969.

3. N. S. Kovar, R. P. Kovar and G. P. Bonner, Planet Space Sci. 17, 143 (1968).

4. R. P. Kovar, "Light Scattering by Large Ice Particles," paper presented at Symposium for Optical Contamination in Space, August 1969.

5. G. Newkirk, Planet Space Sci. 15, 1267 (1967).

6. H. C. Van de Hulst, Light Scattering by Small Particles, Wiley & Sons, New York, (1957).

7. J. L. Weinberg, Annals Astro Phys. 27, 201 (1964).

TABLE I

SPACECRAFT PARAMETERS

Spacecraft	h(km)	dm/dt (gm/sec)	R_o (cm)	M_s (gm/cm^2)
Gemini 3	160	4.2×10^{-3}	2×10^{2}	1.5×10^{-12}
Gemini 11	300	1.4×10^{-2}	2×10^{2}	5.1×10^{-12}
Apollo	300	3×10^{-2}	2×10^{2}	1×10^{-11}
ATM	400-500	1×10^{-1}	3×10^{2}	1×10^{-10}

FIGURES

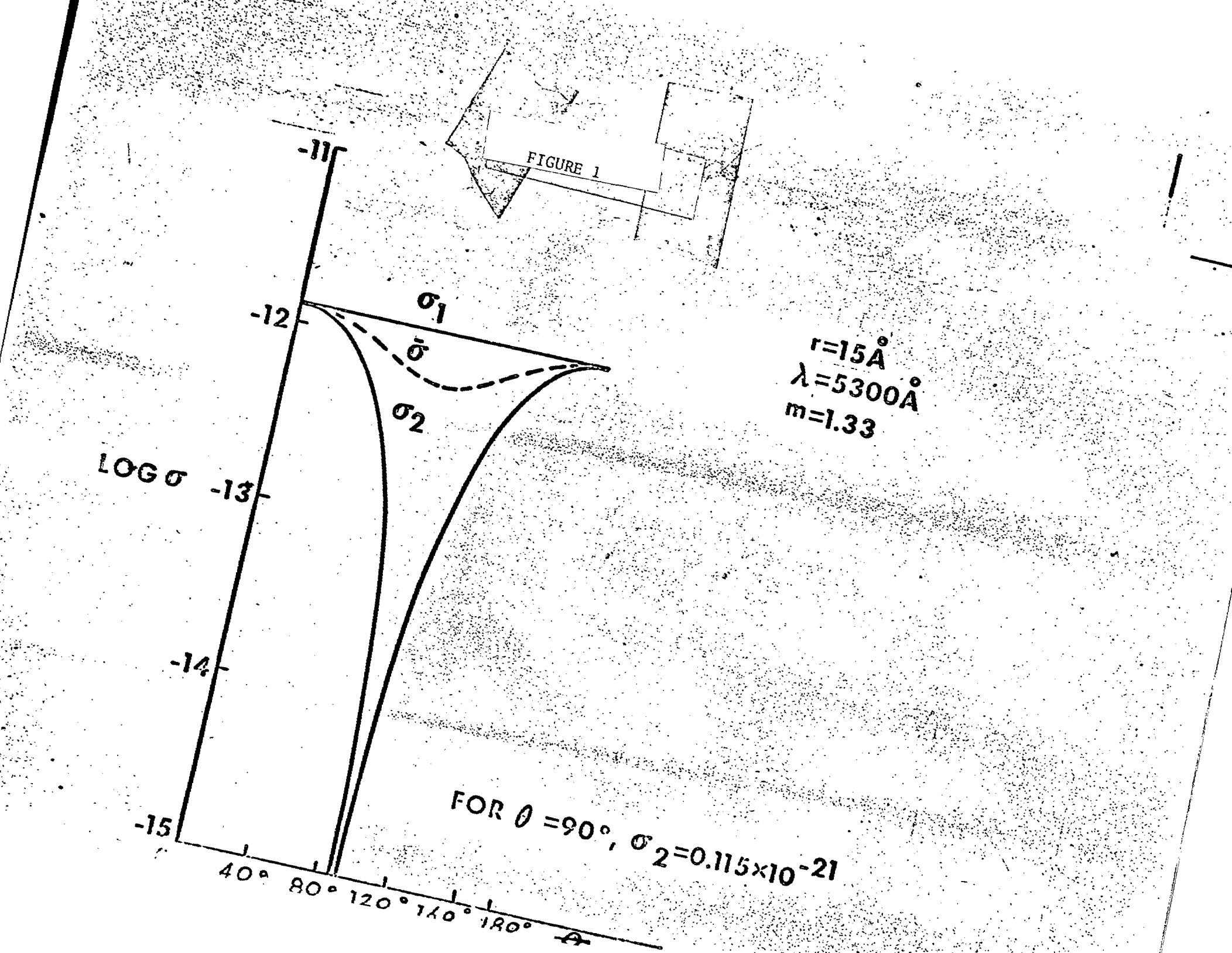
FIGURE 1
-11
-12
-13
-14
-15
LOG σ
σ1
σ̄
σ2
r=15Å
λ=5300Å
m=1.33
FOR θ =90°, σ2=0.115×10-21
40°
80°
120°
140°
180°
θ

FIGURE 2

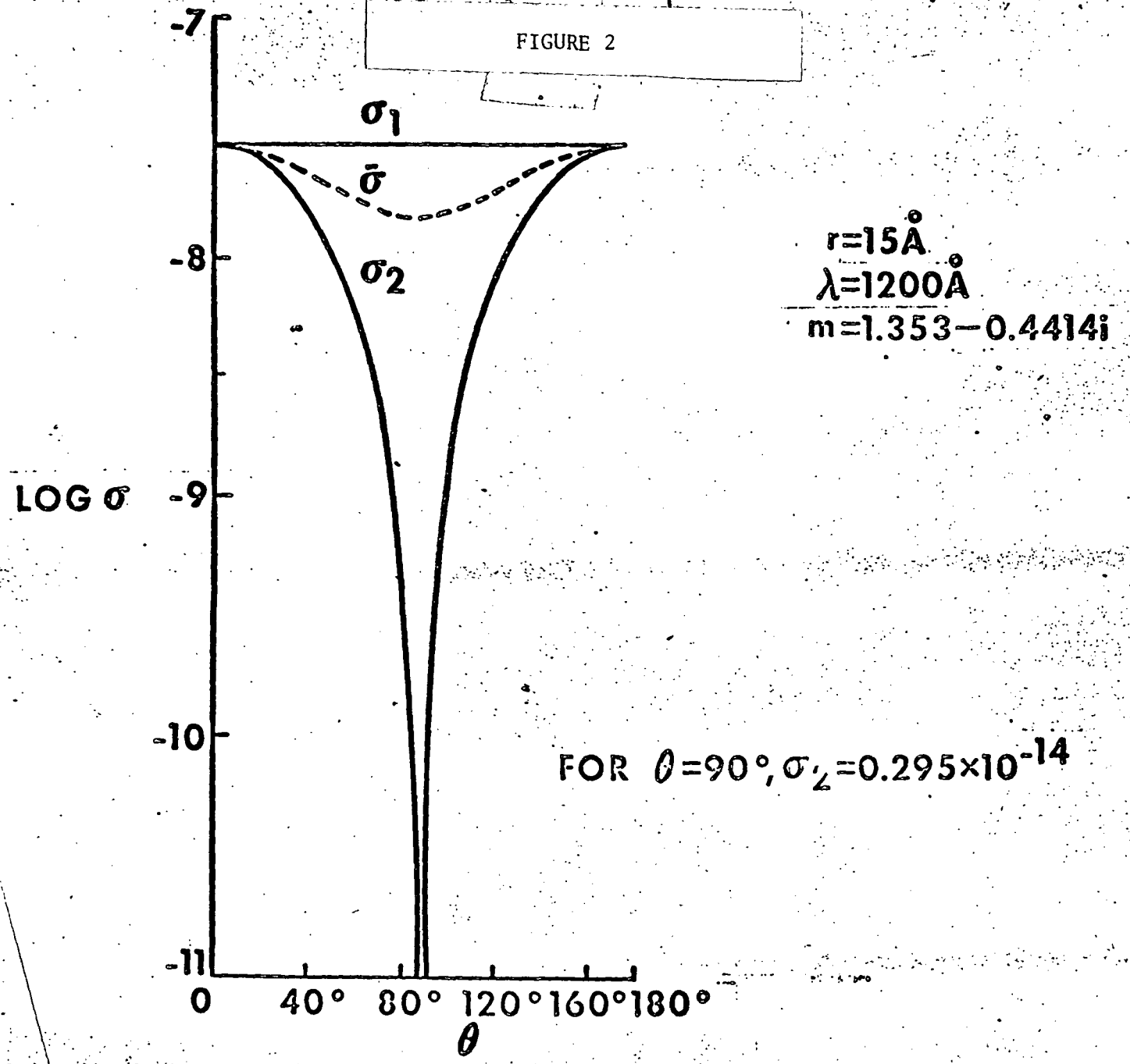

r=15Å
λ=1200Å
m=1.353−0.4414i

FOR $\theta=90°, \sigma_{\perp}=0.295\times10^{-14}$

FIGURE 3

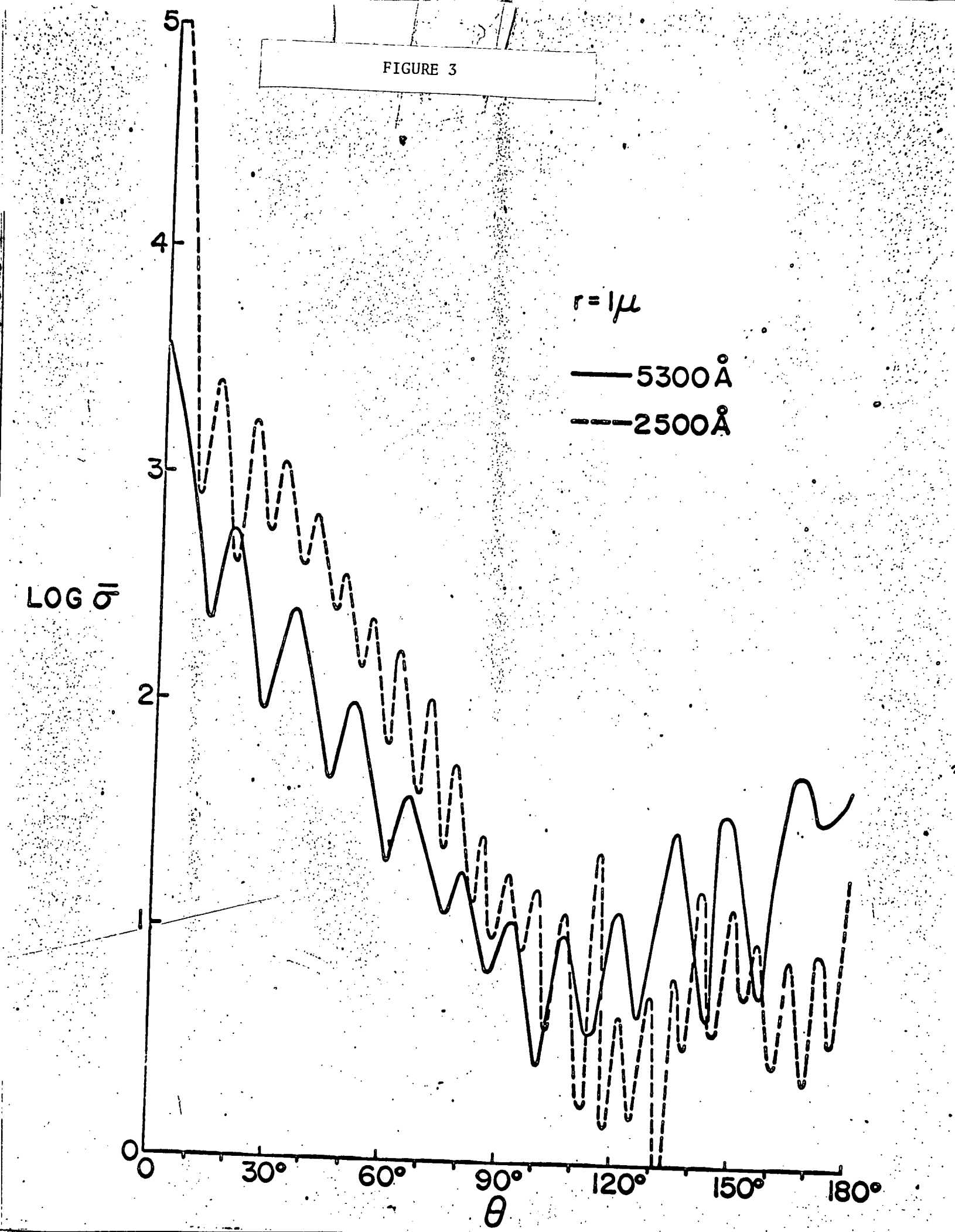
5
4
3
2
1
0
LOG $\bar{\sigma}$
$r = 1\mu$
5300Å
2500Å
0
30°
60°
90°
120°
150°
180°
θ

FIGURE 4

MIE SCATTERING FUNCTION

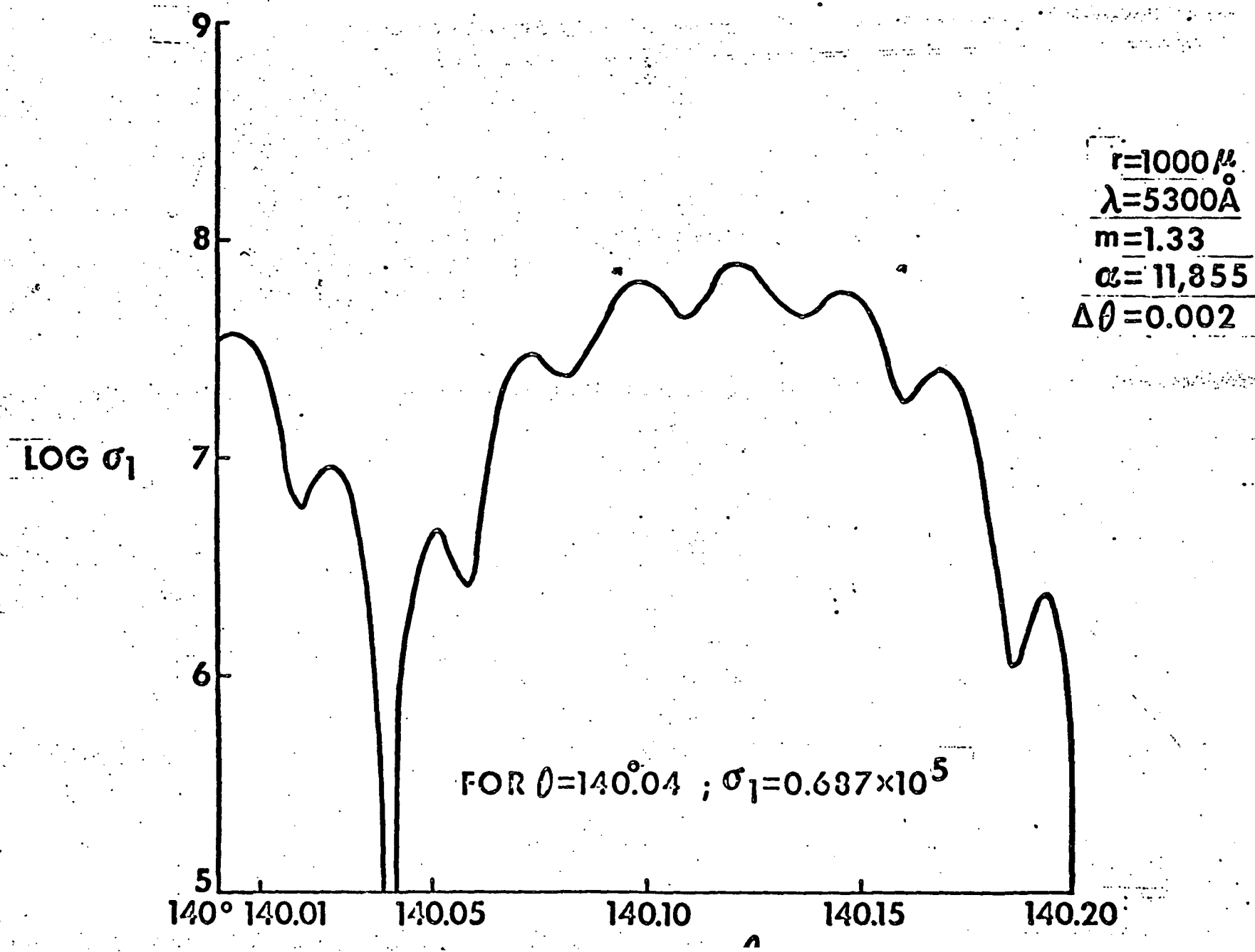

FIGURE 5

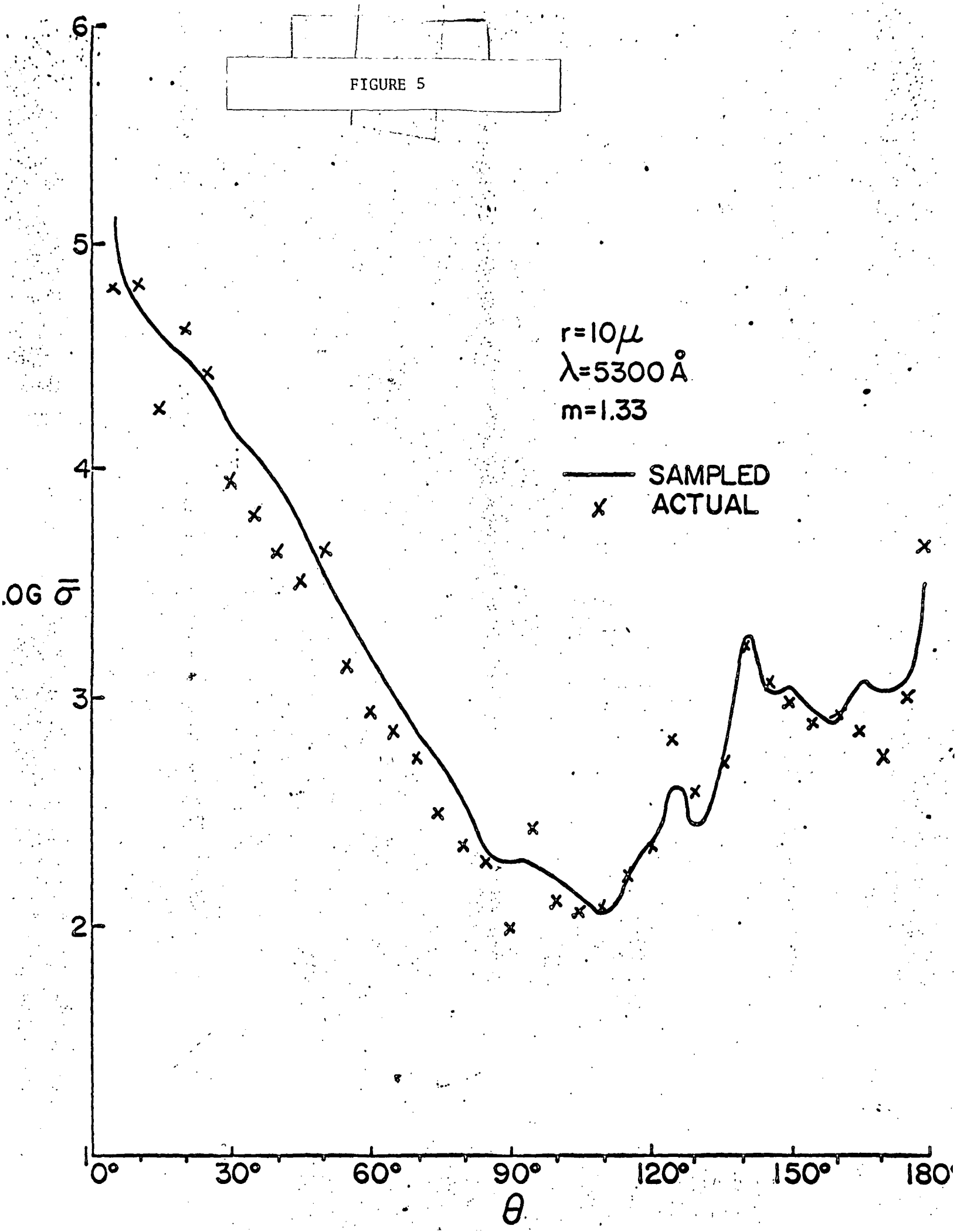
6
5
4
3
2
1
.0G σ̄
r=10μ
λ=5300 Å
m=1.33
SAMPLED
ACTUAL
0°
30°
60°
90°
120°
150°
180
θ

FIGURE 6

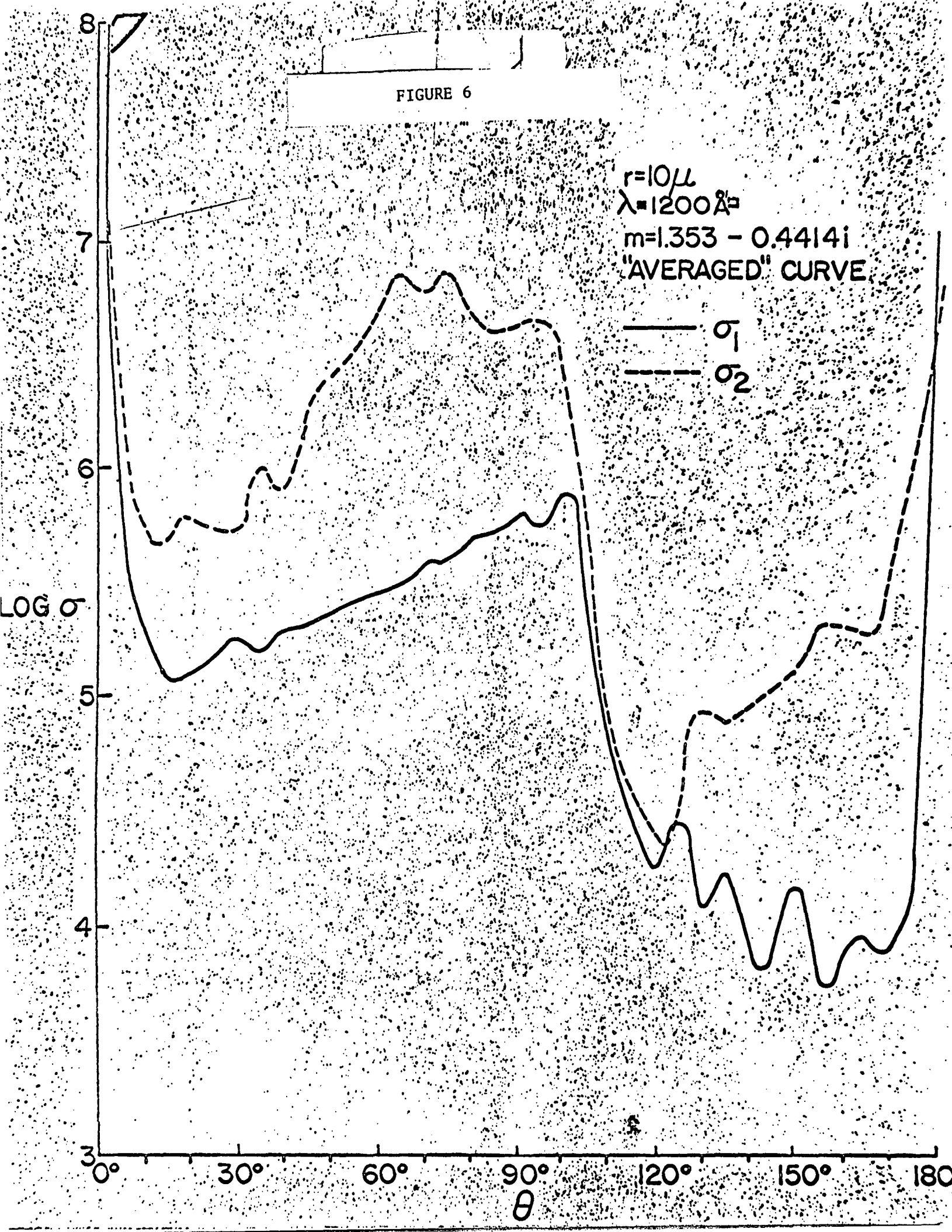
r=10μ
λ=1200Å
m=1.353 - 0.4414i
"AVERAGED" CURVE
σ1
σ2
LOG σ
8
7
6
5
4
3
0°
30°
60°
90°
120°
150°
180
θ

FIGURE 7

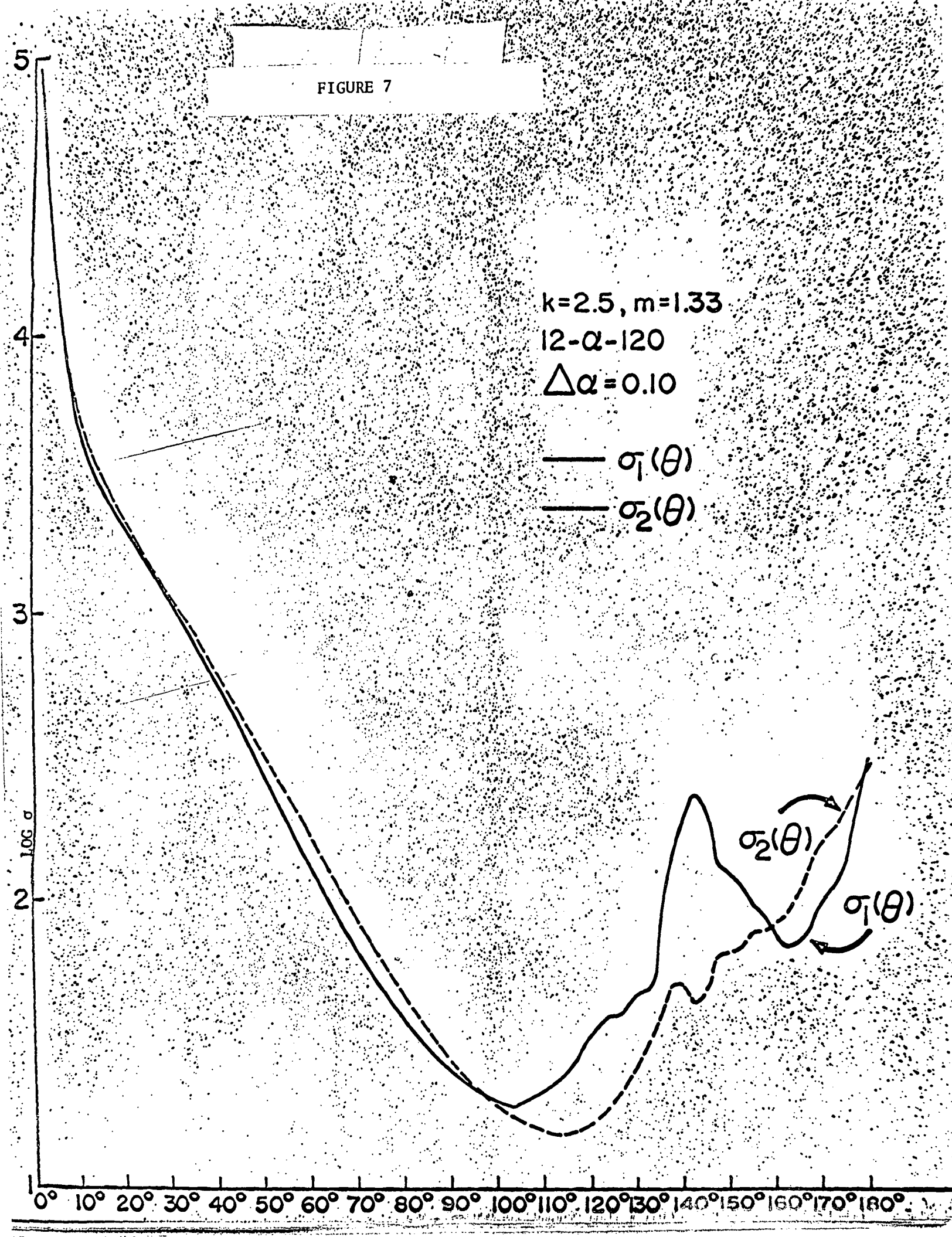
k=2.5, m=1.33
12-α-120
Δα=0.10
σ1(θ)
σ2(θ)
σ2(θ)
σ1(θ)
LOG σ
5
4
3
2
1
0° 10° 20° 30° 40° 50° 60° 70° 80° 90° 100° 110° 120° 130° 140° 150° 160° 170° 180°

FIGURE 8

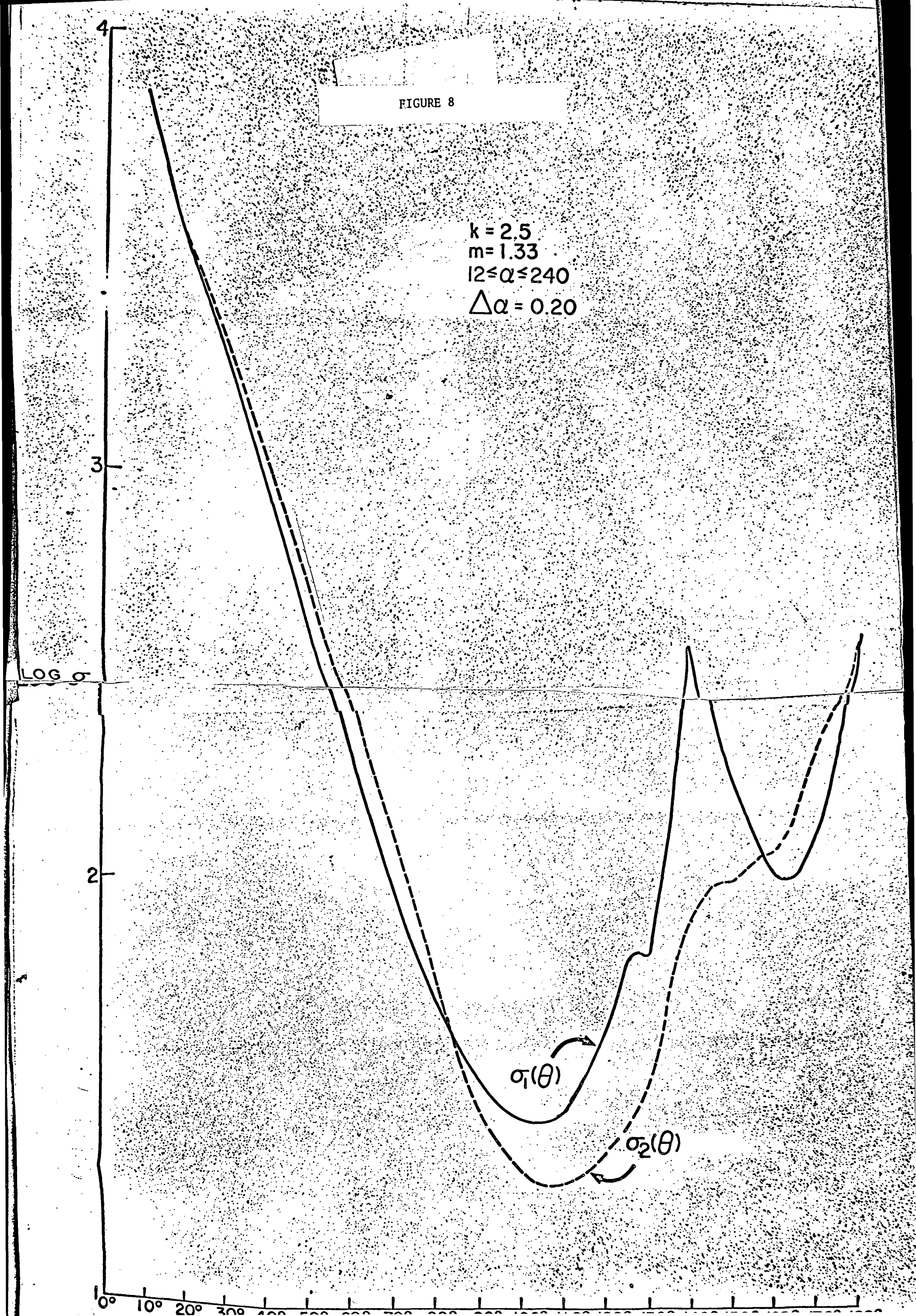
k = 2.5
m = 1.33
12 ≤ α ≤ 240
Δα = 0.20
4
3
2
1
LOG σ
$\sigma_1(\theta)$
$\sigma_2(\theta)$
0°
10°
20°
30°

FIGURE 9

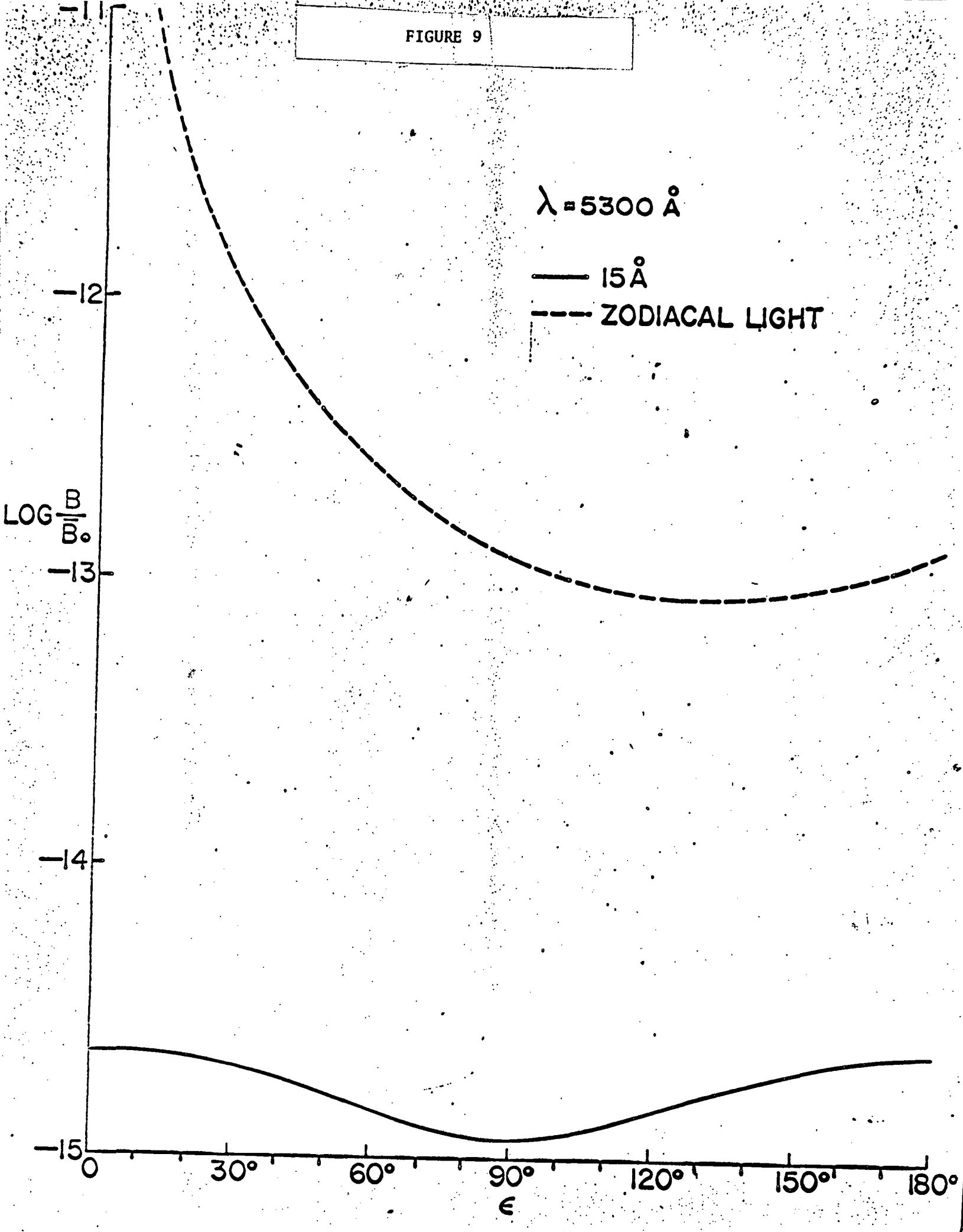
λ = 5300 Å
15 Å
ZODIACAL LIGHT
LOG B/B₀
-11
-12
-13
-14
-15
0
30°
60°
90°
120°
150°
180°
ε

FIGURE 10

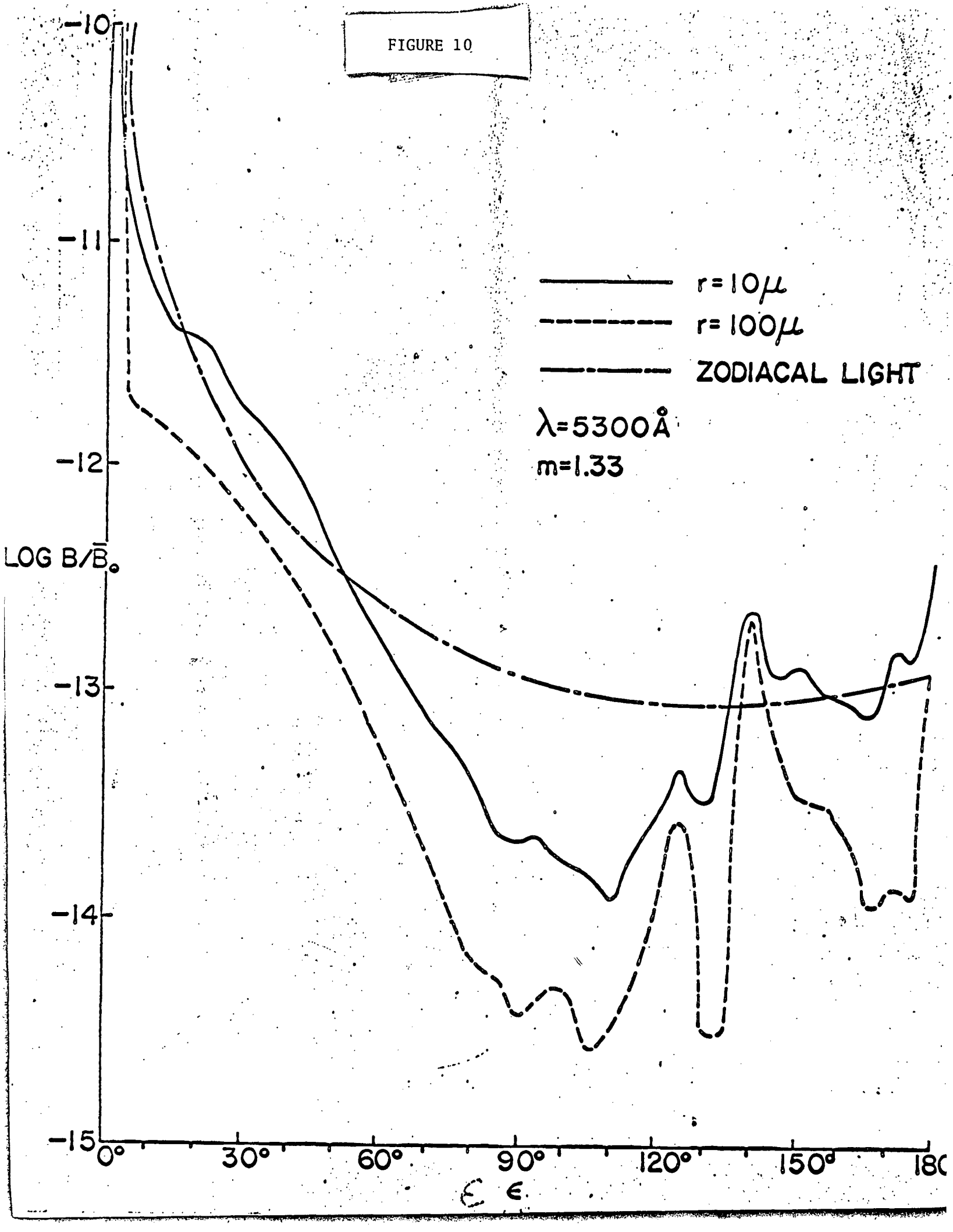
-10
-11
-12
-13
-14
-15
LOG B/B₀
r=10μ
r=100μ
ZODIACAL LIGHT
λ=5300Å
m=1.33
0°
30°
60°
90°
120°
150°
180
ε ε

FIGURE 11

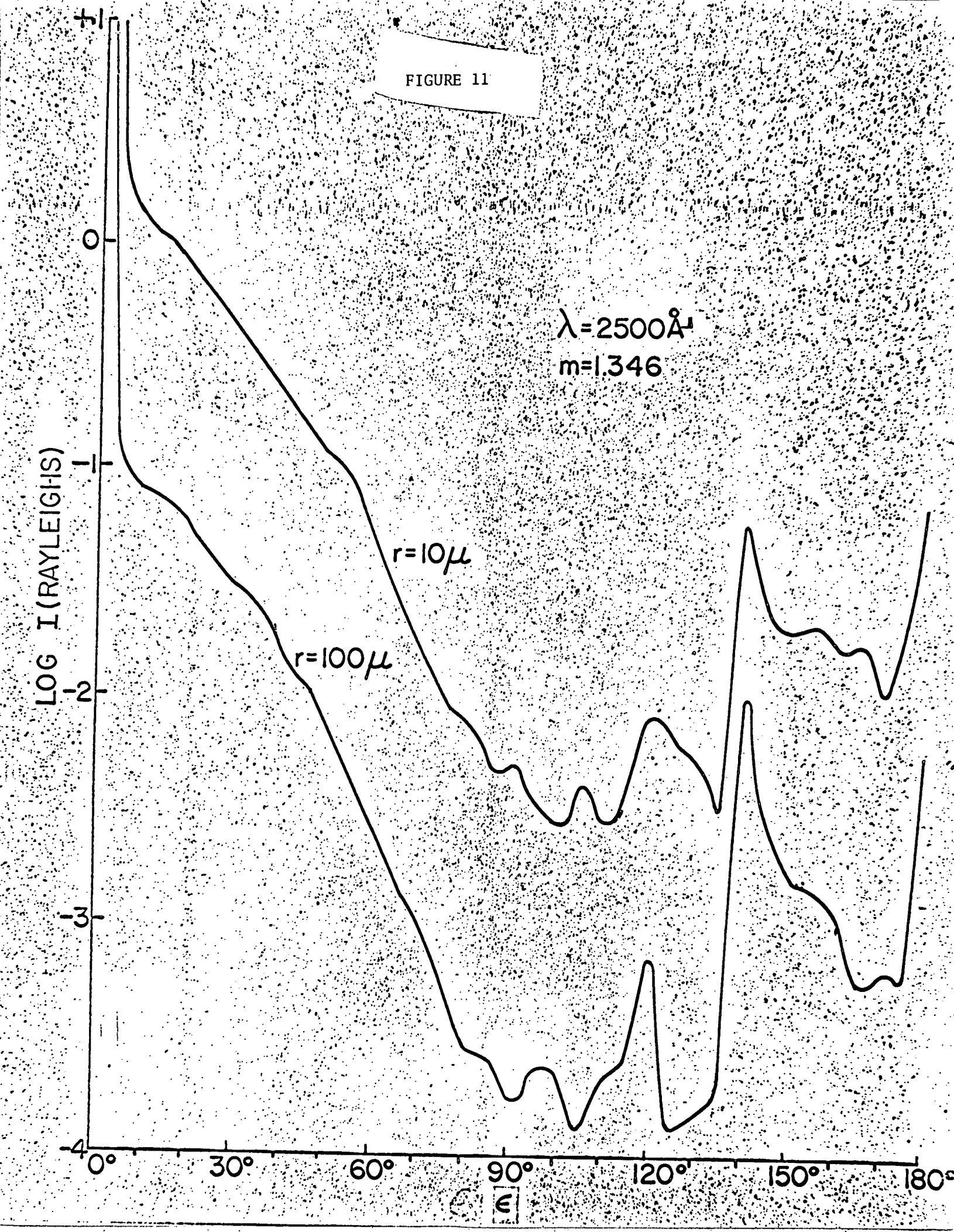
λ=2500Å
m=1.346
r=10μ
r=100μ
LOG I (RAYLEIGHS)
+1
0
-1
-2
-3
-4
0°
30°
60°
90°
120°
150°
180°
ε

FIGURE 12

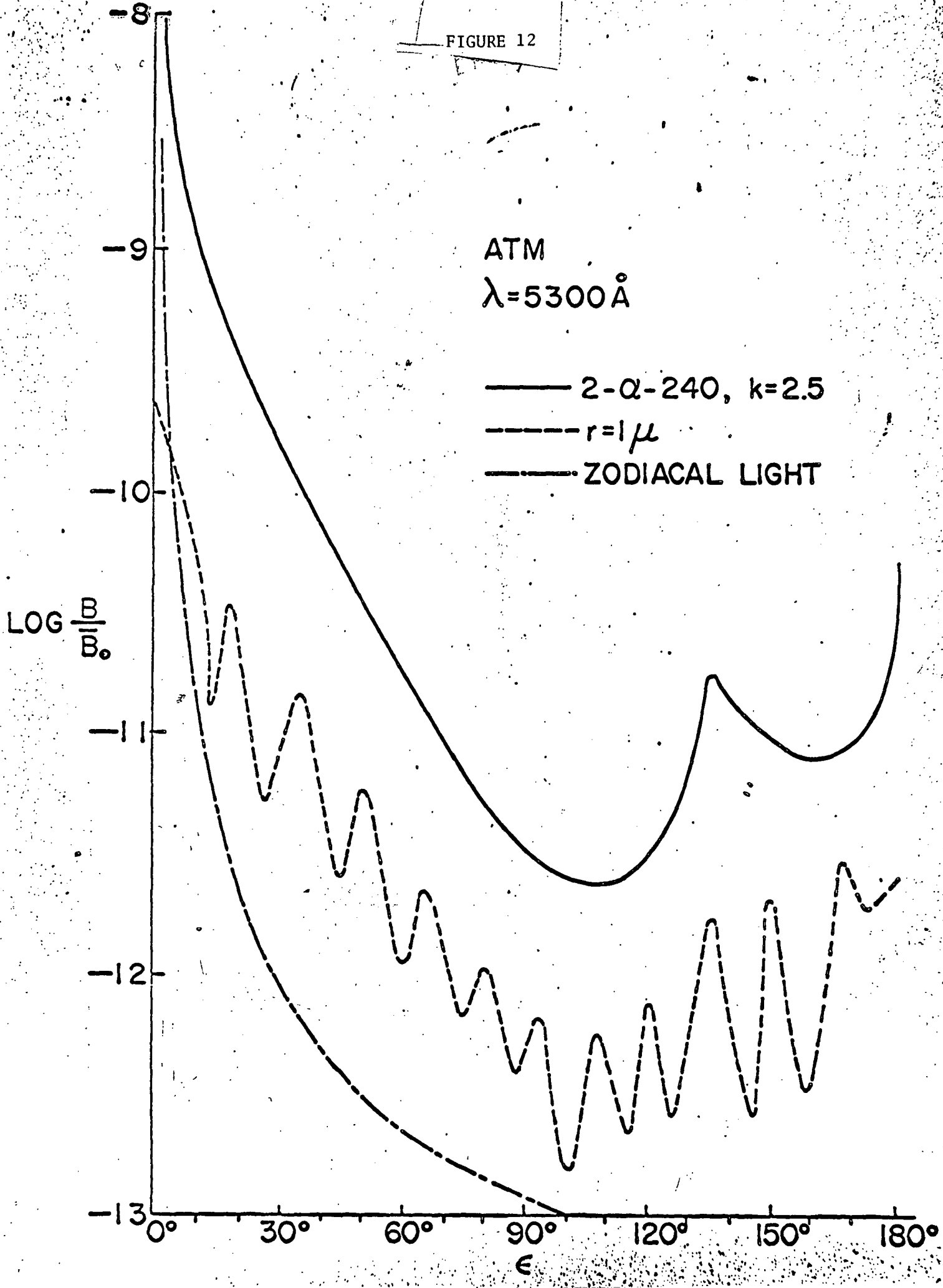
ATM
λ=5300Å
2-α-240, k=2.5
r=1μ
ZODIACAL LIGHT
LOG B/B₀
-8
-9
-10
-11
-12
-13
0°
30°
60°
90°
120°
150°
180°
ε

FIGURE 13

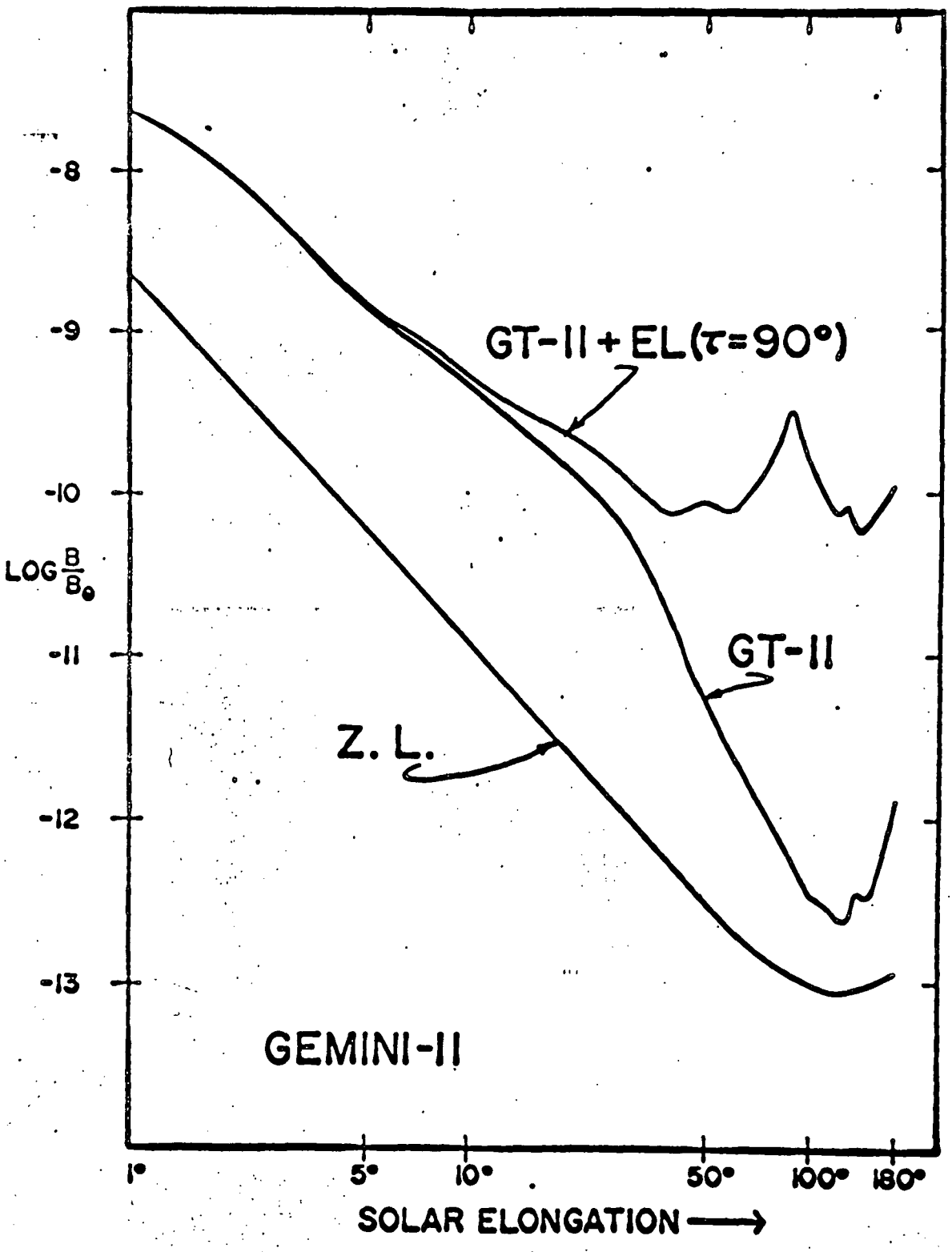
-8
-9
-10
-11
-12
-13
LOG B/B⊙
GT-11 + EL(τ=90°)
GT-11
Z. L.
GEMINI-11
1°
5°
10°
50°
100°
180°
SOLAR ELONGATION ⟶

FIGURE 14

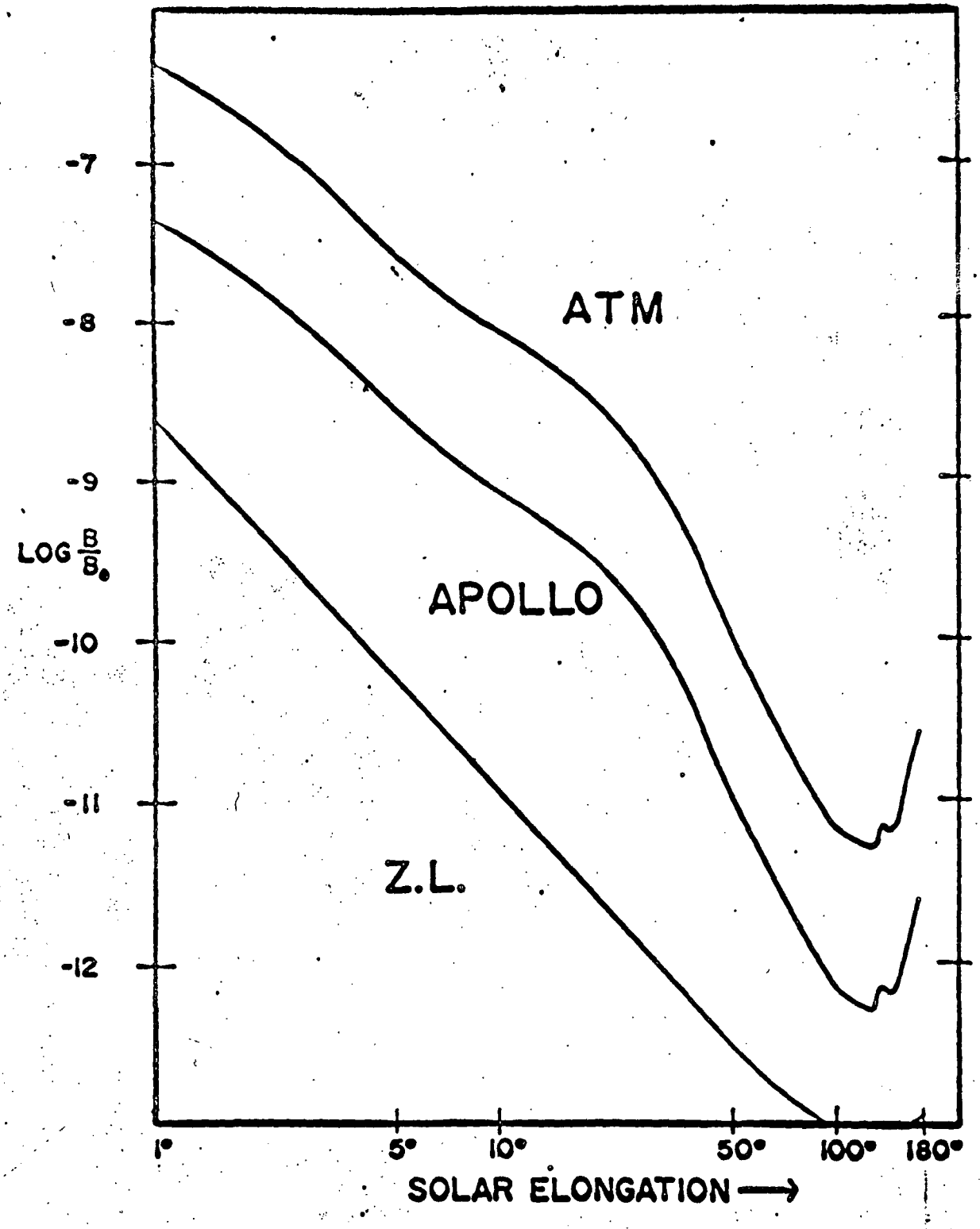
-7
-8
-9
-10
-11
-12
LOG B/B₀
ATM
APOLLO
Z.L.
1°
5°
10°
50°
100°
180°
SOLAR ELONGATION ⟶

APPENDICES

APPENDIX A

Individual Scattering Functions

λ(A°)	$r(\mu)$
5300	15×10^{-4}, 1, 10, 20, 100, 200, 1000, 10,000
2500	15×10^{-4}, 1, 10, 100, 1000, 10,000
2000	15×10^{-4}, 10
1800	15×10^{-4}, 10
1700	15×10^{-4}, 10, 100, 1000
1600	15×10^{-4}, 10, 100, 1000
1500	15×10^{-4}, 10, 100, 1000
1400	15×10^{-4}, 10, 100, 1000
1300	15×10^{-4}, 10, 100, 1000
1200	15×10^{-4}, 1, 10, 1000
1100	15×10^{-4}, 10, 100, 1000
1000	15×10^{-4}, 10, 100, 1000

APPENDIX B

Selected Scattering Functions for a Range of Particle Size*

m	α_1	α_2	k
1.30	1	6	2, 3, 4
	2	12	2.5, 3, 4
	2	240	2.5
	12	30	2.5, 3
	30	60	2.5
	60	90	2.5
	40	120	2.5
	150	180	2.5
1.340	1.396	55.85	4
1.249-0.0472i	0.038	0.077	0
	0.698	1.396	0
	0.077	3.084	4
1.27-1.37i	2	2	2.5
	12	30	2.5
	60	90	2.5

*These results represent only a limited sampling of the scattering functions computed for a column of material for particles of varying size. Results are available for other indices of refraction and for a wide range in increments of α and of θ. In all cases a particle distribution, $n(r) \propto r^{-k}$, was assumed. (The contractor will, upon request, make available any computed data.)